RSC Advances

PAPER

View Article Online
View Journal | View Issue

Check for updates

Cite this: *RSC Adv.*, 2020, **10**, 2453

Synthesis and characterization of thermoresponsive ZIF-8@PNIPAm-*co*-MAA microgel composites with enhanced performance as an adsorption/release platform†

Juan A. Allegretto, [ab] Juan M. Giussi, [a] Sergio E. Moya, [c] Omar Azzaroni *[a] and Matias Rafti *[a]

Received 20th November 2019
Accepted 9th January 2020

DOI: 10.1039/c9ra09729e

rsc.li/rsc-advances

Composite materials featuring a synergic combination of interesting properties such as stimuli responsiveness and tailored porosity are highly appealing due to their multiple possible applications. We hereby present an example which brings together such features by using poly(*N*-isopropyl-acrylamide)-derived thermo-responsive microgels and Zn-based Metal Organic Framework (MOF) ZIF-8, capable of selective adsorption. Such a composite was obtained by including methacrylic acid as a co-monomer in the microgel, in order to position carboxylic acid moieties within the polymeric matrix, which *via* preconcentration of MOF precursors would trigger confined heterogeneous nucleation. The highly integrated composite obtained features thermoresponsivity and permanent porosity. Methylene blue adsorption/desorption experiments were performed, revealing a dramatic enhancement of its cargo capacity together with an increased release efficiency.

Open Access Article. Published on 14 January 2020. Downloaded on 2/10/2026 8:36:32 PM.
This article is licensed under a Creative Commons Attribution-NonCommercial 3.0 Unported Licence.

Introduction

In the last few decades, functional organic–inorganic composite materials have attracted a great deal of attention due to the multiple possibilities arising from a synergic combination of its constituents.[1,2] Examples of such synergy were reported in the recent literature; *e.g.*, composites built from polymers and metallic nanoparticles (NPT) were shown to feature stimuli-responsiveness (towards electric fields, ionic strength, temperature or pH variations), thus allowing interesting applications.[3–6] From the vast palette of stimuli-responsive polymeric materials, microgels have often been employed due to their chemical versatility and straightforward synthesis, which typically yields monodisperse distributions of micrometer-sized particles.[7,8] Among the most popular applications of microgels, examples dealing with controlled nucleation of crystalline solids,[9] separations,[10] biomedicine,[11,12] and drug delivery[13] can be mentioned. In particular, poly(*N*-isopropyl-acrylamide)-PNIPAm-microgels constitute a suitable thermoresponsive platform for many of the above-discussed examples.[14] Responsiveness of PNIPAm arises from a change in the relative strength of solvent–monomer and monomer–monomer interactions; *i.e.*, at low temperatures a solvated (swollen) microgel configuration dominates, while as temperature increases, solvent-monomer interactions become weaker, ultimately triggering a transition into desolvated (unswollen) state. The characteristic temperature for such transition is known as the lower critical solution temperature or LCST (typically ≈30 °C for PNIPAm).[15–17] LCST and other key features of PNIPAm microgels (*e.g.*; size, exposed chemical moieties, pH responsiveness, or surface charge) are highly dependent on polymer structure and can be modified by including different co-monomers (*e.g.*; methacrylic acid (MAA) for pH-responsiveness and surface charge modulation).[18–20] Quite recently, ionic microgels have been used as platforms for synthesis of metallic NPT; a two-step procedure consisting in diffusion of metal precursors followed by chemical treatment,[21,22] yield composites featuring photoluminescence, modified magnetic properties or surface-enhanced Raman scattering.[23–26]

An appealing approach for the modification of the above discussed organic–inorganic composites would be; *e.g.*, to replace metallic NPT with other nanostructures. Recent examples deal with the possibility of using SiO_2 nanoparticles as cores from which microgels can be grown in order to achieve core–shell structures that retain the key feature of volume phase transition.[27,28] An interesting further development of such a strategy could be to replace the SiO_2 core with a different

[a]*Instituto de Investigaciones Fisicoquímicas Teóricas y Aplicadas (INIFTA), Departamento de Química, Facultad de Ciencias Exactas, Universidad Nacional de La Plata, CONICET, Calle 64 y Diag. 113, 1900 La Plata, Argentina. E-mail: azzaroni@inifta.unlp.edu.ar; mrafti@quimica.unlp.edu.ar*

[b]*Universidad Nacional de San Martin (UNSAM), San Martín, Argentina*

[c]*CIC biomaGUNE, Paseo de Miramón 182, Donostia-San Sebastián, 20014, Spain*

† Electronic supplementary information (ESI) available: Experimental details, data processing details, NMR, and TEM results. See DOI: 10.1039/c9ra09729e

Open Access Article. Published on 14 January 2020. Downloaded on 2/10/2026 8:36:32 PM.
This article is licensed under a Creative Commons Attribution-NonCommercial 3.0 Unported Licence.

material capable of conferring porosity and/or tailored affinity for targeted adsorbates. Metal Organic Frameworks or MOFs are ideal candidates for this purpose, given that suitable methods for synthesizing such composites become available. MOFs can be best described as spatially extended crystalline porous solids, composed of metallic ion centers (or clusters containing metallic ions), non-covalently linked by multidentate organic molecules.[29,30]

Although not extensively explored, there are some recent examples of polymer-MOF composites.[31] Namely, the synthesis of poly(methyl methacrylate) and polystyrene composites with water-sensitive Zn-based MOF-5 (which results in an increased stability towards hydrolysis, without compromising available pore volume),[32,33] the use of surface-grafted MOF particles integrated with PNIPAm as thermoresponsive emulsifiers and drug-delivery platforms,[34,35] and the use of hydrogels containing MOFs for adsorption from aqueous environments.[36] Inspired by such examples and the already reported possibility of combining colloidal templates and nanostructures,[37,38] we envisioned the possibility of synthesizing well dispersed polymer-MOF composites following a straightforward approach; *i.e.*, by using pre-designed microgel particles featuring moieties able to trigger MOF heterogeneous nucleation, which would add microporosity to the thermoresponsive polymer. The main drive for such interest was to explore the possibility of attaining further control over adsorption–desorption processes, colloidal stability, and the integration of further components in the composite (*e.g.*; metallic nanoparticles) for additional functionality. In order to explore this concept, we have chosen an archetypal member of the Zeolitic Imidazolate Framework (ZIFs) MOF subclass, known as ZIF-8 (composed by Zn^{2+} ions tetrahedrally coordinated by 2-methylimidazolate anionic linkers) and extensively used in photocatalysis,[39,40] biocatalysis,[41,42] and drug delivery[43,44] applications. ZIF-8 features sodalite-like topology with BET surface areas up to $\approx 1900\ m^2\ g^{-1}$, relatively high thermal/chemical stability, and eminently hydrophobic micropores (1.16 nm diameter and 0.34 nm pore window).[45] Thorough characterization of the composite was carried, confirming the presence of a well-integrated microporous ZIF-8 phase within the polymer matrix. Afterwards, experiments oriented to demonstrate the suitability of the composite for adsorption/desorption of selected analytes were conducted with methylene blue (MB) aqueous solutions.[46] Such experiments show that the obtained composite features a synergic combination of its components and is capable of outperforming ZIF-8 MOF as adsorbent platform; *i.e.*, it was observed a three-fold increase for its maximum loading capacity, and a ten-fold increase of its release efficiency.

Experimental

Materials

N-Isopropylacrylamide (NIPAm, $M_w = 113.16\ g\ mol^{-1}$), *N*,*N*′-methylene-bis-acrylamide (BIS, $M_w = 154.17\ g\ mol^{-1}$), ammonium persulfate (APS, $M_w = 228.20\ g\ mol^{-1}$), methacrylic acid (MAA, $M_w = 86.09\ g\ mol^{-1}$), zinc nitrate hexahydrate (ZnN), 2-methylimidazole (HmIm), sodium chloride, methylene blue (MB) and anhydrous methanol were purchased from Sigma-Aldrich and used without further purification. Ultrapure Milli-Q water (18.24 MΩ cm) was used for all the aqueous solutions.

Microgel synthesis

1.358 g of NIPAm and 0.043 g of *N*,*N*′-methylene-bis-acrylamide (BIS) were dissolved in 100 mL of Milli-Q water (1 : 0.023 molar ratio) and heated under stirring to 70 °C while purging with N_2 in a 250 mL three-neck round-bottom flask. Then, 0.148 g of MAA were added for a final 1 : 0.143 molar ratio of NIPAm : MAA, under continuous stirring. Next, 0.046 g of APS dissolved in 1 mL Milli-Q water at room temperature were added to the reaction mixture (for a final 1 : 0.017 NIPAm : APS molar ratio). After 4 hours of synthesis, a microgel dispersion was obtained and then purified by (3×) sequential centrifugation/re-dispersion procedure followed by freeze-drying.

ZIF-8 synthesis

ZIF-8 MOF was synthesized by mixing equal volumes of methanolic 25 mM $Zn(NO_3)_2$ –ZnN– and 50 mM 2-methylimidazole-HmIm-solutions at 25 °C. After 1 hour reaction time, dispersions obtained were centrifuged at 7000 rpm for 30 minutes and re-dispersed three times in NaCl 5 mM solution. Concentrations were determined *via* dry weight with TGA to be 1.6 ± 0.1 mg mL^{-1}.

ZIF-8@microgel synthesis

Freeze-dried microgel samples were dispersed using ZIF-8 metallic precursor ZnN 25 mM solution (final concentration 1 mg mL^{-1} microgel) and kept one week under controlled temperature (4 °C) in order to ensure complete pre-concentration of the metal ion in the polymeric matrix. Afterward, a 50 mM methanolic solution of HmIm linker was added in order to yield a final (1 : 2) Zn : HmIm stoichiometric molar ratio. After 1 hour synthesis, dispersions obtained were centrifuged at 6000 rpm for 30 minutes in a Heraeus Biofuge 22R with an HFA 1494 rotor, and re-dispersed in NaCl 5 mM three times. Moderate ionic strengths were needed while manipulating microgels in aqueous environments in order to reach its full swollen state.[19] As presented in ESI†, synthesized materials exposed to aqueous environments for 5 months were found to remain stable, supporting the possibility of re-use in cyclic procedures.

Characterization techniques used

Dynamic Light Scattering (DLS) measurements were carried using a Zetasizer Nano-ZS90 (Malvern Instruments Ltd.), and Wide-Angle X-ray Scattering (WAXS) in a Xeuss 1.0 HR SAXS/WAXS, XENOCS, Grenoble setup (INIFTA, project "Nanopymes", EuropeAid/132184/D/SUP/AR-Contract 331-896, UNLP-CONICET) with a microfocus X-ray source and Pilatus 100K detector (Dectris, Switzerland, distance sample-detector: 97.95 mm). ^{1}H-NMR (Nuclear Magnetic Resonance, Brucker 500 MHz) experiments were performed using deuterated methanol.

 This journal is © The Royal Society of Chemistry 2020

Open Access Article. Published on 14 January 2020. Downloaded on 2/10/2026 8:36:32 PM.
This article is licensed under a Creative Commons Attribution-NonCommercial 3.0 Unported Licence.

Thermogravimetric Analysis (TGA) experiments were carried using Pt pans under 60 mL min^{-1} N_2 flow; all samples were kept at 100 °C until constant weight to ensure proper drying, and then the temperature was ramped (5 °C min^{-1}) up to 900 °C (TGA Q500, TA Instruments). Surface area determination was carried with an ASAP 2020 HD88 surface area and porosity analyzer (Micromeritics). TEM (Transmission Electron Microscopy) images were obtained using JEM 1200EX II (Jeol) apparatus using (when required) phosphotungstic acid negative staining as a contrast agent. A UV-Vis spectrometer Ocean Optics USB4000 spectrometer was employed to perform the UV-Vis spectra presented. Raman vibrational spectra were obtained with an i-Raman Plus (B&W Tek inc.) apparatus, using a 785 nm light source. Integration time was set to 5000 ms, with a time average of 100 and a 50% laser intensity.

Results and discussion

Microgel and ZIF-8@microgel synthesis and characterization

By means of free-radical precipitation copolymerization, thermoresponsive poly(*N*-isopropyl-acrylamide-*co*-methacrylic acid) or poly(NIPAm-*co*-MAA) microgels with 81% NIPAm-19% MAA composition were obtained (see ESI† for further details about synthesis procedures and NIPAm : MAA ratio calculation from NMR).[19] Taking advantage of the affinity between carboxylate moieties and Zn^{2+} ions, microgels were used as soft preconcentration platforms, which then allowed for confined ZIF-8 growth (hereafter referred as ZIF-8@microgel).[47] Reaction time needed for composite synthesis was determined by mixing methanolic solutions of ZIF-8 precursors at 25 °C while continuously monitoring hydrodynamic diameter (D_h) *via* DLS. The final stage of particle growth is attained after 1 hour reaction time ($D_h \approx 400$ nm, see Fig. S1†), and therefore the same value was used for ZIF-8@microgel synthesis. As presented in Fig. 1a, D_h corresponding to bare microgel particles (≈739 nm) is slightly smaller than ZIF-8@microgel (≈795 nm). The fact that no additional particles with different size distribution were observed suggest that heterogeneous nucleation within the microgel is greatly enhanced over homogeneous ZIF-8 nucleation.[20] Further evidence of the suggested confined growth can be obtained from DLS autocorrelation curves (Fig. 1a, inset). Bare microgel and ZIF-8@microgel diffusion coefficients were determined to be 1.09 μm^2 s^{-1} to 0.33 μm^2 s^{-1}, respectively, which is a strong indication of increasingly compact particles compatible with ZIF-8 integration to the polymeric matrix. Thermogravimetric analysis (TGA) was employed for determination of the ZIF-8/microgel relative amounts (see Fig. 1b), using onset and magnitude of thermal events registered, a 50% w/w composition can be derived.

As presented in Fig. 2a, the sequence of events leading to composite formation were characterized by different techniques: firstly, Zn^{2+} ions complexation by MAA groups was probed throughout Raman vibrational spectroscopy, as displayed in Fig. 2b. Spectra obtained for bare ZIF-8, bare microgel, and ZIF-8@microgel composite, feature characteristic vibrational modes; namely, 175 cm^{-1} (Zn–N stretching mode) and 686 cm^{-1} (HmIm ring Pickering mode). As shown in the

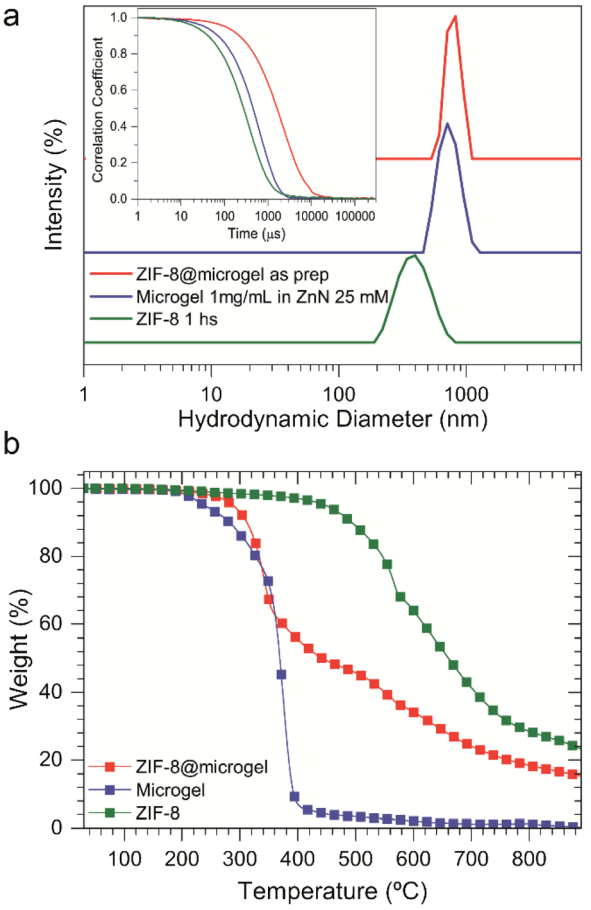

Fig. 1 (a) Hydrodynamic diameter (D_h) (intensity distribution) of ZIF-8 particles after one-hour synthesis and comparison with 1 mg mL^{-1} microgel dispersion in 25 mM $Zn(NO_3)_2$ methanolic solution, and the as-prepared ZIF-8@microgel dispersion. Inset: autocorrelation curves. (b) Thermogravimetric experiments for quantification of ZIF-8 and microgel content in the composite.

enlarged wavenumber region, bare microgel presents a composed signal arising from NIPAm and MAA contributions (NIPAm signal at 1650 cm^{-1} and MAA signal at 1710 cm^{-1}), however, for ZIF-8@microgel composite only the signal corresponding to NIPAm is present. The absence of MAA contribution supports the proposed partial coordination of Zn^{2+} with carboxylic moieties present in the microgel. Additional evidence was provided through pH values of native dispersions, see ESI.† Secondly, ZIF-8 network formation was probed by WAXS. Diffractograms displayed at Fig. 2c evidence high crystallinity for the MOF present in the composite, with no significant differences with the results obtained for bare ZIF-8.

In order to explore the close integration achieved between microgel and MOF, ^{1}H-NMR experiments were carried; while signals obtained coincide with those expected for ZIF-8 and microgel (see Fig. S2†), nuclear Overhauser effect spectroscopy (NOESY) reveals a clear coupling between imidazolic signals and those rising from the microgel network. As presented in Fig. 3, coupling between 1 ppm signal arising from MAA methylene groups and NIPAm moieties, and 3.8 ppm and

Open Access Article. Published on 14 January 2020. Downloaded on 2/10/2026 8:36:32 PM.
This article is licensed under a Creative Commons Attribution-NonCommercial 3.0 Unported Licence.

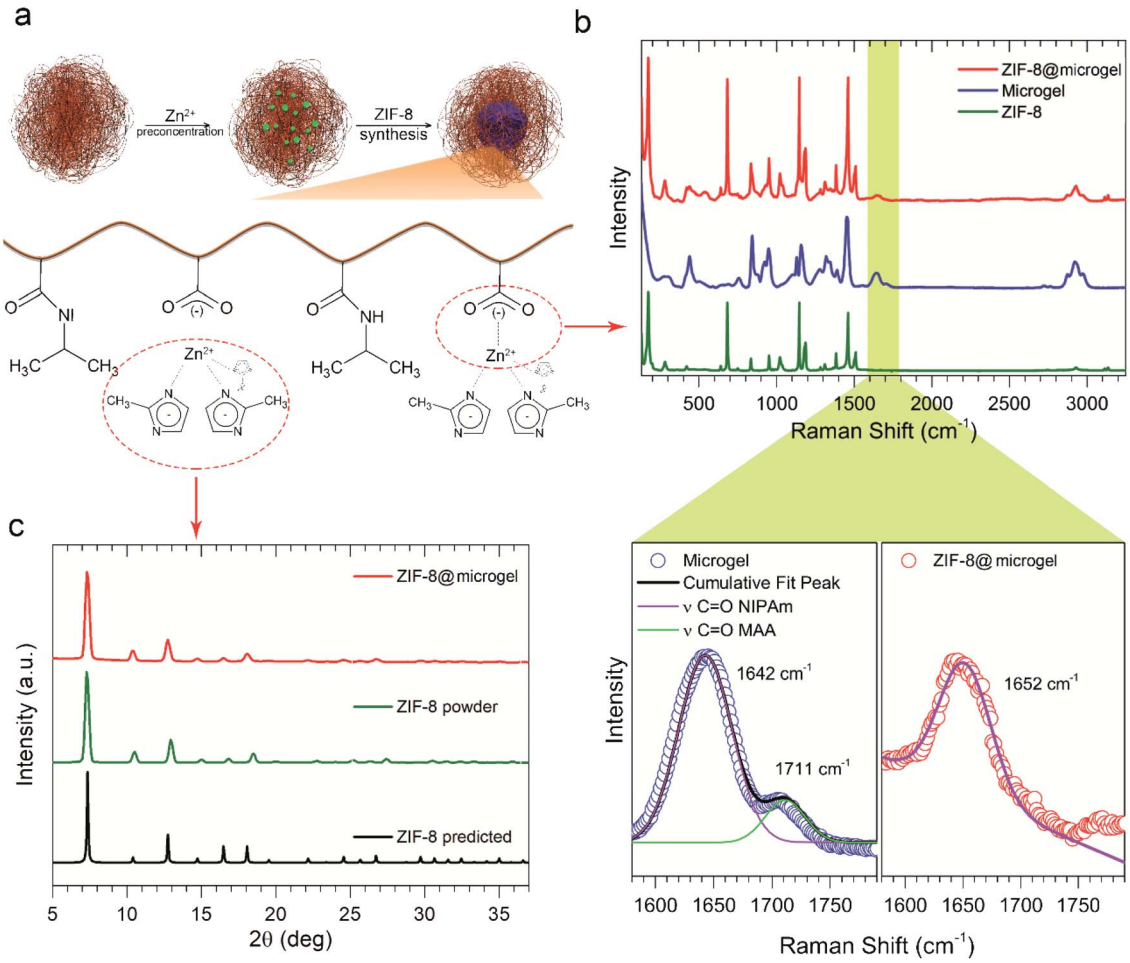

Fig. 2 (a) Schematic representation of Zn^{2+} ions preconcentration by MAA monomers from the microgel matrix and the subsequent ZIF-8 formation. (b) Raman vibrational spectra for ZIF-8 powder, dry microgel, and dry ZIF-8@microgel. Highlighted wavenumber region where C=O peaks appear. (c) Diffraction patterns from WAXS experiments.

7.1 ppm signals corresponding to imidazole ring, rules out the possibility of phase segregation, since coupling is mediated by dipole–dipole interactions between non-bonded moieties, only possible if separation lengths are lower than 6 Å.

Having established the presence of ZIF-8 in the microgel, experiments oriented to determine the presence of porosity and surface area inherent to MOF were carried. Results of N_2 adsorption isotherms at 77 K are presented in Fig. 4; a steep increase in the adsorbed volume typical of IUPAC type I isotherms together with BJH-derived pore size distribution maximum at 1.1 nm (Fig. 4, inset) were observed.[45] Determined BET surface area was 632 ± 5 $m^2\ g^{-1}$ (with no significant difference with Langmuir analysis, 666 ± 6 $m^2\ g^{-1}$). Having in mind that microgel contribution to the surface area can be considered negligible, and using TGA-determined weight composition (50%, see Fig. 1b), it can be assumed that ZIF-8 porosity (~1200 $m^2\ g^{-1}$) remains available when assembled in the composite (see ESI† for further details on the calculations).

Morphology and mesoscopic organization of the synthesized materials were studied with transmission electron microscopy (TEM). The use of a staining agent (phosphotungstic acid) in order to confer electronic contrast was necessary only for bare microgel due to the electron-dense MOF phase present in the composite. TEM images are presented in Fig. 5. As can be seen, the presence of ZIF-8 across the microgel particle is evident, supporting the proposed confined nucleation and growth process and the structural integration of the composite (for size distribution analysis, see ESI†).

Microgel and ZIF-8@microgel thermoresponsive behaviour

The question of whether the thermoresponsive behavior of the microgel is affected or not by the presence of ZIF-8 in the composite was addressed by DLS experiments. Hydrodynamic diameters corresponding to microgel and ZIF-8@microgel dispersions prepared in 5 mM NaCl were compared (concentrations determined by dry weight were 1.73 ± 0.01 and 1.7 ± 0.2 mg mL^{-1} respectively); results are displayed in Fig. 6. At 25 °C (swollen state) D_h determined values were quite similar for both materials; while at 45 °C (collapsed state) a notorious difference appeared. The collapse of the composite microparticles is hindered by the presence of the less-compressible ZIF-8

 This journal is © The Royal Society of Chemistry 2020

Open Access Article. Published on 14 January 2020. Downloaded on 2/10/2026 8:36:32 PM.
This article is licensed under a Creative Commons Attribution-NonCommercial 3.0 Unported Licence.

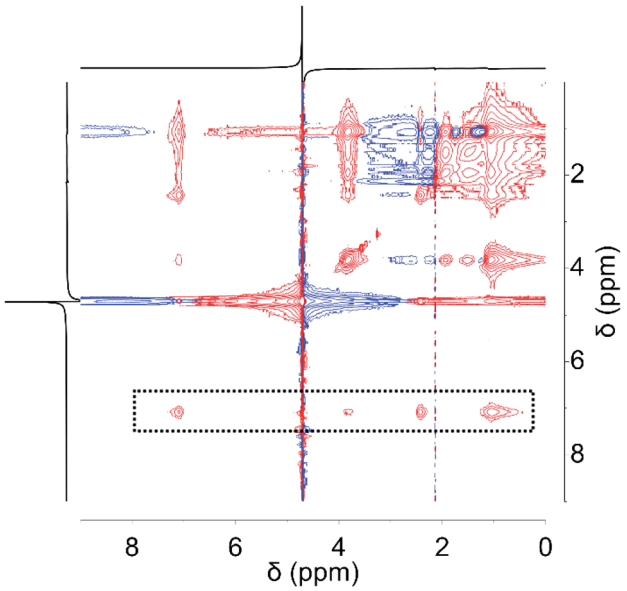

Fig. 3 Nuclear Overhauser effect spectroscopy (NOESY) analysis for ZIF-8@microgel composite material. Dashed area marks features arising from coupling between imidazolate and microgel signals.

phase, causing a difference of approx. 160 nm (as already reported for similar metallic NPT@microgel composites).[28,48]

Methylene blue (MB) adsorption and desorption

Having characterized the integration between MOF and polymeric matrix in the composite, its chemical structure, morphology, and thermal responsiveness; we focused on exploring possible uses as adsorption–desorption platforms, considering the demonstrated available porosity present. For this end, methylene blue (MB) aqueous stock solutions were exposed to homogeneous dispersions of ZIF-8, bare microgel, and ZIF-8@microgel composite (see Scheme 1a). In order to ensure equilibrium state, contact time used was 48 h; afterward,

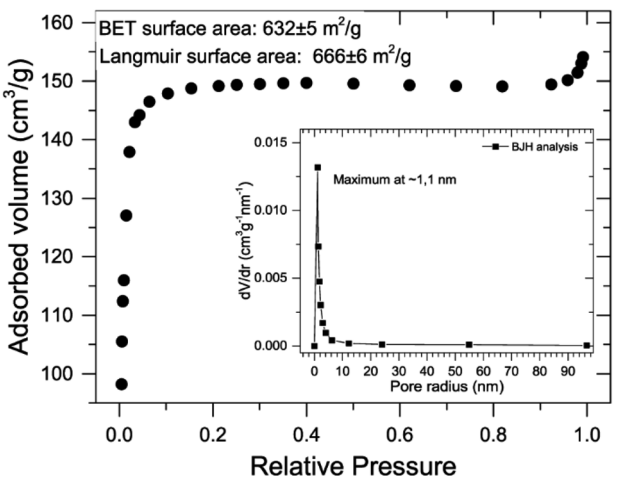

Fig. 4 N_2 adsorption isotherm for ZIF-8@microgel composite. Inset: pore size distribution by BJH method.

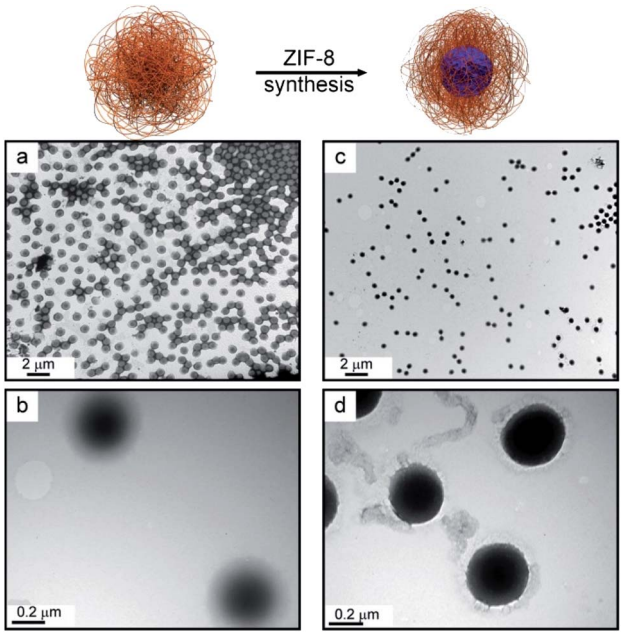

Fig. 5 Transmission Electron Microscopy (TEM) images of (a) stained bare microgel particles at 8k and (b) non-stained microgel particles at 120k magnification. ZIF-8@microgel particles at (c) 8k and (d) 120k magnification, both without staining agent.

suspensions were centrifuged, and equilibrium MB concentrations were determined by UV-Vis spectroscopy (see Scheme 1b). Adsorbent containing MB was then re-dispersed in NaCl 5 mM and left 48 h in order to determine MB release, which was quantified as a percentage (release efficiency, % RE) of the MB originally adsorbed in the considered support (further details on the procedure followed can be found at ESI†).

Low-concentration limit adsorption isotherms obtained are presented in Fig. 7; interestingly, and despite the differences

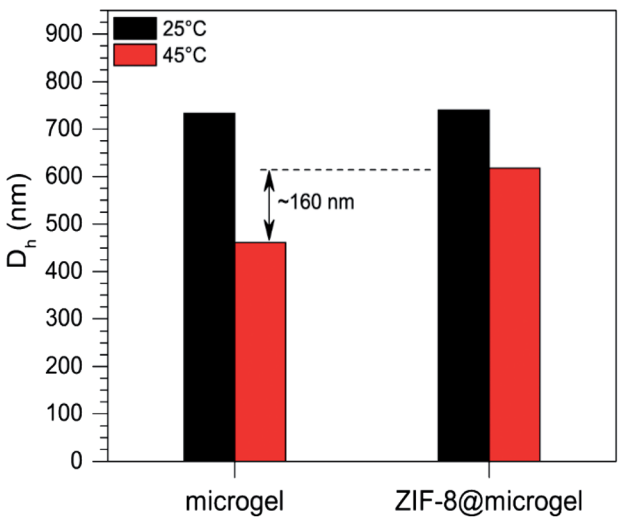

Fig. 6 Size transition comparison for microgel and ZIF-8@microgel particles between 25 °C and 45 °C as measured from DLS experiments.

Open Access Article. Published on 14 January 2020. Downloaded on 2/10/2026 8:36:32 PM.
This article is licensed under a Creative Commons Attribution-NonCommercial 3.0 Unported Licence.

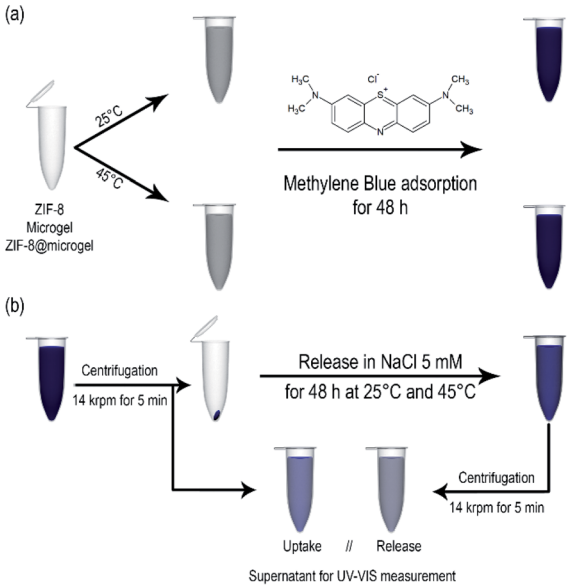

Scheme 1 MB adsorption (a) and release (b) for ZIF-8, microgel, and ZIF-8@microgel.

between Langmuir model ideal adsorbent and the complex composite solid hereby considered, all the measured isotherms can be reasonably well fitted, with some minor differences for ZIF-8@microgel at 25 °C. Langmuir model, from which parameters characterizing adsorption were obtained, can be expressed as follows:

$$Q_e = \frac{Q_0 K_L C_e}{1 + K_L C_e}$$

where C_e and Q_e are the determined equilibrium values for MB concentration in the liquid phase and mass loading (adsorbed amount) in the adsorbent; while Q_0 and K_L are the values obtained from Langmuir model fitting, corresponding to high-concentration limit adsorbed amount and the adsorption constant, related to the Gibbs free energy of adsorption according to $\Delta G^0 = RT \ln(K_L)$.

A comparison of Q_0 values obtained for the different isotherms fitted to experimental data is presented in Fig. 8. It is worth mentioning that Q_0 obtained for ZIF-8 suspensions can be considered as a lower-limit value, given that the expected particle aggregation in aqueous environments in aqueous environments would hinder adsorbate access to the total available porosity.

Fig. 8 clearly shows that ZIF-8@microgel adsorbent outperforms both bare microgel and ZIF-8, even considering what could be expected from a simple linear combination of the contributions. In order to assess the potential of ZIF-8@microgel composite for; *e.g.*, drug-delivery applications, the release of adsorbed MB was tested using adsorbent phase exposed to MB solutions corresponding to initial concentrations of 0.04 mg mL^{-1} (see ESI† for details). Release efficiency (RE), was calculated for each adsorbent as the amount of MB released with respect to the initial amount adsorbed (relevant contact time values were used for release experiments; *i.e.*, 48 h), see Fig. 9. Values obtained suggest that, while contact time is clearly not sufficient for reaching desorption equilibrium, there is an evident improvement on the RE for the composite. ZIF-8 RE is quite small at both temperatures compared with bare microgel and ZIF-8@microgel, which show considerable temperature dependence. Bare ZIF-8 is a strong adsorbent ($\Delta H_{ads} = -13.7$ kJ mol^{-1} as derived from Gibbs free energy of adsorption); however, a marked RE increase can be observed for both, microgel and ZIF-8@microgel, which amounts to approx. a 10-fold increase and almost a 3-fold increase when comparing with values corresponding to 25 °C and 45 °C respectively. Such marked temperature dependence can be understood in terms of structural changes occurring in the microgel structure when transitions between collapsed and swollen states occur. In the collapsed microgel (45 °C),

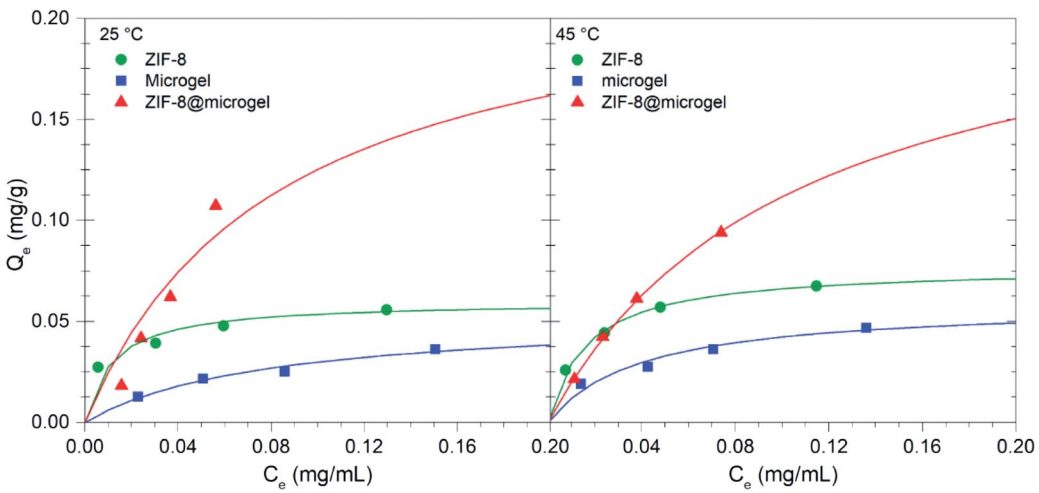

Fig. 7 Equilibrium isotherms for MB adsorption and Langmuir fits using bare microgel, ZIF-8 and ZIF-8@microgel adsorbent at 25 °C (left, swollen state) and 45 °C (right, collapsed state). Full lines correspond to Langmuir fits.

 This journal is © The Royal Society of Chemistry 2020

Open Access Article. Published on 14 January 2020. Downloaded on 2/10/2026 8:36:32 PM.
This article is licensed under a Creative Commons Attribution-NonCommercial 3.0 Unported Licence.

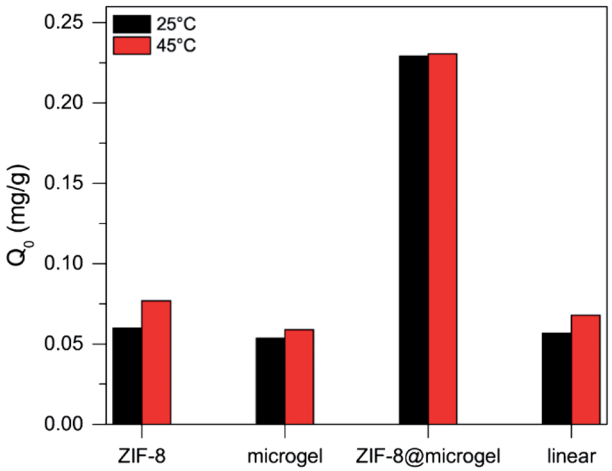

Fig. 8 Comparison of Q_0 parameters as calculated from Langmuir isotherm fit at 25 °C and 45 °C. Linear refers to a Q_0 calculated value assuming the weight composition derived from TGA experiments and linear contributions of both components.

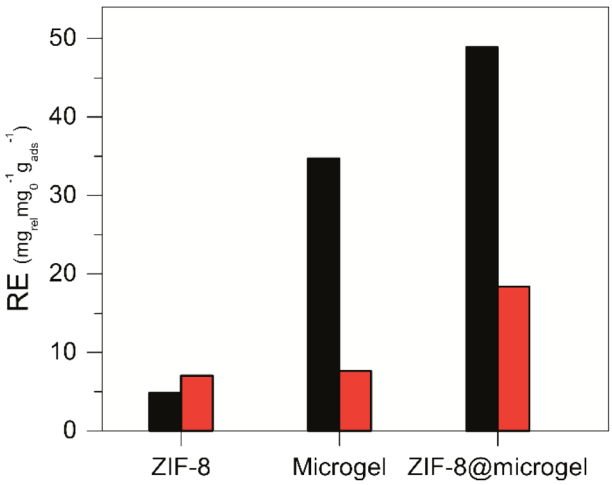

Fig. 9 Release Efficiency – RE after 48 h, using initial MB concentrations $C_0 = 0.04$ mg mL^{-1} for ZIF-8, microgel, and ZIF-8@microgel adsorbent.

NIPAm–NIPAm hydrophobic interactions prevail and provoke particle core to become increasingly hydrophobic, together with segregation of free MAA moieties towards particle surface, this generates an increased negative surface charge.[49] Both effects cause an increased affinity between MB and the microgel resulting thus in a lower RE value for the collapsed state (45 °C). Regarding the enhanced release observed for the composite at 25 °C, it can be rationalized by considering an equilibrium between MB adsorbed in the microporous environment provided by ZIF-8 and MB adsorbed in regions corresponding to free microgel chains (responsible for temperature triggered transitions). As MB desorbs from polymeric environment towards solution, ZIF-8-adsorbed MB (which act as a reservoir) is continuously released to compensate such release.

Conclusions

We hereby report for the first time on the use of Poly(*N*-isopropyl-acrylamide-*co*-methacrylic acid) (poly(NIPAm-*co*-MAA)) thermoresponsive microgel as a macromolecular template for ZIF-8 confined heterogeneous nucleation. The strategy followed was to synthesize a microgel featuring MAA moieties, which can act as Zn^{2+} partial coordination sites, and *via* supersaturation effect, trigger confined MOF heterogeneous nucleation, both phenomena proved by Raman spectroscopy and WAXS experiments. The highly integrated (as observed *via* NMR) ZIF-8@microgel synthesized material retains both high surface area and thermal responsiveness.

MB adsorption/desorption experiments reveal a clear synergy when comparing ZIF-8@microgel performance *versus* what could be expected from the combined contributions of bare ZIF-8 and microgel separately. ZIF-8 was demonstrated to be a strong adsorbent but a poor delivery platform due to a very low release efficiency (RE). The use of ZIF-8@microgel composite was shown to cause an overall improvement of adsorption/desorption performance. The observed effect of temperature variations on RE (*i.e.*, RE-25 °C > RE-45 °C) for the composite allows foreseeing potential applications for its use as drug release platform. The general principles hereby described can be applied with little modification to diverse MOFs and stimuli-responsive polymeric materials, which we believe will open the path for many interesting applications of such nanocomposites.

Conflicts of interest

There are no conflicts to declare.

Acknowledgements

M. R., J. M. G., and O. A. are CONICET staff members. J. A. A. wants to acknowledge Jorge L. Llanos, Edgardo A. Fertitta and Ethel S. Flores for the help and discussion regarding TGA and N_2 uptake experiments, Lorena Cortez for graphical material, and CONICET for a doctoral scholarship.

Notes and references

1 M. Faustini, L. Nicole, E. Ruiz-hitzky and C. Sanchez, History of Organic–Inorganic Hybrid Materials: Prehistory, Art, Science, and Advanced Applications, *Adv. Funct. Mater.*, 2018, **28**, 1704158.
2 P. Gomez-Romero, Hybrid Organic–Inorganic Materials—In Search of Synergic Activity, *Adv. Mater.*, 2001, **13**, 163–174.
3 M. A. C. Stuart, W. T. S. Huck, J. Genzer, M. Müller, C. Ober, M. Stamm, G. B. Sukhorukov, I. Szleifer, V. V. Tsukruk, M. Urban, F. Winnik, S. Zauscher, I. Luzinov and S. Minko, Emerging applications of stimuli-responsive polymer materials, *Nat. Mater.*, 2010, **9**, 101–113.
4 A. Shiotani, T. Mori, T. Niidome, Y. Niidome and Y. Katayama, Stable incorporation of gold nanorods into *N*-isopropylacrylamide hydrogels and their rapid shrinkage

Open Access Article. Published on 14 January 2020. Downloaded on 2/10/2026 8:36:32 PM. This article is licensed under a Creative Commons Attribution-NonCommercial 3.0 Unported Licence.

induced by near-infrared laser irradiation, *Langmuir*, 2007, **23**, 4012–4018.

5 M. Nguyen, N. Felidj and C. Mangeney, Looking for Synergies in Molecular Plasmonics through Hybrid Thermoresponsive Nanostructures, *Chem. Mater.*, 2016, **28**(11), 3564–3577.

6 Z. Qian and D. S. Ginger, Reversibly Reconfigurable Colloidal Plasmonic Nanomaterials, *J. Am. Chem. Soc.*, 2017, **139**, 5266–5276.

7 J. B. Thorne, G. J. Vine and M. J. Snowden, Microgel applications and commercial considerations, *Colloid Polym. Sci.*, 2011, **289**(5–6), 625–646.

8 S. Nayak and L. Andrew Lyon, Soft nanotechnology with soft nanoparticles, *Angew. Chem., Int. Ed.*, 2005, **44**, 7686–7708.

9 Y. Diao, M. E. Helgeson, A. S. Myerson, T. A. Hatton, P. S. Doyle and B. L. Trout, Controlled Nucleation from Solution Using Polymer Microgels, *J. Am. Chem. Soc.*, 2011, **133**, 3756–3759.

10 H. Kaşgöz, S. Özgümüş and M. Orbay, Modified polyacrylamide hydrogels and their application in removal of heavy metal ions, *Polymer*, 2003, **44**, 1785–1793.

11 B. R. Saunders, N. Laajam, E. Daly, S. Teow, X. Hu and R. Stepto, Microgels: from responsive polymer colloids to biomaterials, *Adv. Colloid Interface Sci.*, 2009, **147–148**, 251–262.

12 M. K. Nguyen and E. Alsberg, Bioactive factor delivery strategies from engineered polymer hydrogels for therapeutic medicine, *Prog. Polym. Sci.*, 2014, **39**, 1235–1265.

13 J. Ramos, A. Imaz, J. Callejas-Fernández, L. Barbosa-Barros, J. Estelrich, M. Quesada-Pérez and J. Forcada, Soft nanoparticles (thermo-responsive nanogels and bicelles) with biotechnological applications: from synthesis to simulation through colloidal characterization, *Soft Matter*, 2011, **7**, 5067.

14 J. Pérez-Juste, I. Pastoriza-Santos and L. M. Liz-Marzán, Multifunctionality in metal@microgel colloidal nanocomposites, *J. Mater. Chem. A*, 2013, **1**, 20–26.

15 J. Wu, B. Zhou and Z. Hu, Phase Behavior of Thermally Responsive Microgel Colloids, *Phys. Rev. Lett.*, 2003, **90**, 048304.

16 B. R. Saunders, On the Structure of Poly(*N*-isopropylacrylamide) Microgel Particles, *Langmuir*, 2004, **20**, 3925–3932.

17 S. M. Hashmi and E. R. Dufresne, Mechanical properties of individual microgel particles through the deswelling transition, *Soft Matter*, 2009, **5**, 3682.

18 K. Tauer, D. Gau, S. Schulze, A. Völkel and R. Dimova, Thermal property changes of poly(*N*-isopropylacrylamide) microgel particles and block copolymers, *Colloid Polym. Sci.*, 2009, **287**, 299–312.

19 J. M. Giussi, M. I. Velasco, G. S. Longo, R. H. Acosta and O. Azzaroni, Unusual temperature-induced swelling of ionizable poly(*N*-isopropylacrylamide)-based microgels: experimental and theoretical insights into its molecular origin, *Soft Matter*, 2015, **11**, 8879–8886.

20 M. Rafti, J. A. Allegretto, G. M. Segovia, J. S. Tuninetti, J. M. Giussi, E. Bindini and O. Azzaroni, Metal–organic frameworks meet polymer brushes: enhanced crystalline film growth induced by macromolecular primers, *Mater. Chem. Front.*, 2017, **1**, 2256–2260.

21 K. Akamatsu, M. Shimada, T. Tsuruoka, H. Nawafune, S. Fujii and Y. Nakamura, Synthesis of pH-Responsive Nanocomposite Microgels with Size-Controlled Gold Nanoparticles from Ion-Doped, Lightly Cross-Linked Poly(vinylpyridine), *Langmuir*, 2010, **26**, 1254–1259.

22 J. Zhang, S. Xu and E. Kumacheva, Polymer microgels: reactors for semiconductor, metal, and magnetic nanoparticles, *J. Am. Chem. Soc.*, 2004, **126**, 7908–7914.

23 R. A. Álvarez-Puebla, R. Contreras-Cáceres, I. Pastoriza-Santos, J. Pérez-Juste and L. M. Liz-Marzán, Au@pNIPAM Colloids as Molecular Traps for Surface-Enhanced, Spectroscopic, Ultra-Sensitive Analysis, *Angew. Chem., Int. Ed.*, 2009, **48**, 138–143.

24 L. Wang, X. Zhao, Y. Zhang, W. Zhang, T. Ren, Z. Chen, F. Wang and H. Yang, Fabrication of intelligent poly(*N*-isopropylacrylamide)/silver nanoparticle composite films with dynamic surface-enhanced Raman scattering effect, *RSC Adv.*, 2015, **5**, 40437–40443.

25 L. Tan, J. Liu, W. Zhou, J. Wei and Z. Peng, A novel thermal and pH responsive drug delivery system based on ZnO@PNIPAM hybrid nanoparticles, *Mater. Sci. Eng., C*, 2014, **45**, 524–529.

26 L.-Y. Chen, C.-M. Ou, W.-Y. Chen, C.-C. Huang and H.-T. Chang, Synthesis of Photoluminescent Au ND–PNIPAM Hybrid Microgel for the Detection of Hg^{2+}, *ACS Appl. Mater. Interfaces*, 2013, **5**, 4383–4388.

27 M. Karg, I. Pastoriza-Santos, L. M. Liz-Marzán and T. Hellweg, A versatile approach for the preparation of thermosensitive PNIPAM core–shell microgels with nanoparticle cores, *ChemPhysChem*, 2006, **7**, 2298–2301.

28 M. Karg, S. Wellert, I. Pastoriza-Santos, A. Lapp, L. M. Liz-Marzán and T. Hellweg, Thermoresponsive core–shell microgels with silica nanoparticle cores: size, structure, and volume phase transition of the polymer shell, *Phys. Chem. Chem. Phys.*, 2008, **10**, 6708.

29 S. Li and F. Huo, Metal-organic framework composites: from fundamentals to applications, *Nanoscale*, 2015, **7**, 7482–7501.

30 N. Stock and S. Biswas, Synthesis of Metal-Organic Frameworks (MOFs): Routes to Various MOF Topologies, Morphologies, and Composites, *Chem. Rev.*, 2012, **112**, 933–969.

31 A. Zimpel, T. Preiß, R. Röder, H. Engelke, M. Ingrisch, M. Peller, J. O. Rädler, E. Wagner, T. Bein, U. Lächelt and S. Wuttke, Imparting Functionality to MOF Nanoparticles by External Surface Selective Covalent Attachment of Polymers, *Chem. Mater.*, 2016, **28**, 3318–3326.

32 K. A. McDonald, J. I. Feldblyum, K. Koh, A. G. Wong-Foy and A. J. Matzger, Polymer@MOF@MOF: 'grafting from' atom transfer radical polymerization for the synthesis of hybrid porous solids, *Chem. Commun.*, 2015, **51**, 11994–11996.

33 N. D. H. Gamage, K. A. McDonald and A. J. Matzger, MOF-5-Polystyrene: Direct Production from Monomer, Improved Hydrolytic Stability, and Unique Guest Adsorption, *Angew. Chem., Int. Ed.*, 2016, **55**, 12099–12103.

 This journal is © The Royal Society of Chemistry 2020

Open Access Article. Published on 14 January 2020. Downloaded on 2/10/2026 8:36:32 PM.
This article is licensed under a Creative Commons Attribution-NonCommercial 3.0 Unported Licence.

34 S. Nagata, K. Kokado and K. Sada, Metal–organic framework tethering PNIPAM for ON–OFF controlled release in solution, *Chem. Commun.*, 2015, **51**, 8614–8617.
35 B. Yao, Q.-J. Fu, A.-X. Li, X.-M. Zhang, Y.-A. Li and Y.-B. Dong, A thermo-responsive polymer-tethered and Pd NP loaded UiO-66 NMOF for biphasic CB dechlorination, *Green Chem.*, 2019, **21**, 1625–1634.
36 O. Maan, P. Song, N. Chen and Q. Lu, An *In Situ* Procedure for the Preparation of Zeolitic Imidazolate Framework-8 Polyacrylamide Hydrogel for Adsorption of Aqueous Pollutants, *Adv. Mater. Interfaces*, 2019, **6**(19), 1801895.
37 M.-P. Pileni, The role of soft colloidal templates in controlling the size and shape of inorganic nanocrystals, *Nat. Mater.*, 2003, **2**, 145–150.
38 U. Betke and A. Lieb, Micro-Macroporous Composite Materials - Preparation Techniques and Selected Applications: A Review, *Adv. Eng. Mater.*, 2018, **20**, 1800252.
39 J. Duan, S. Chen and C. Zhao, Ultrathin metal-organic framework array for efficient electrocatalytic water splitting, *Nat. Commun.*, 2017, **8**, 1–7.
40 Y. Zhang, Q. Li, C. Liu, X. Shan, X. Chen, W. Dai and X. Fu, The promoted effect of a metal-organic frameworks (ZIF-8) on Au/TiO_2 for CO oxidation at room temperature both in dark and under visible light irradiation, *Appl. Catal., B*, 2018, **224**, 283–294.
41 X. Wu, J. Ge, C. Yang, M. Hou and Z. Liu, Facile synthesis of multiple enzyme-containing metal–organic frameworks in a biomolecule-friendly environment, *Chem. Commun.*, 2015, **51**, 13408–13411.
42 C. Hou, Y. Wang, Q. Ding, L. Jiang, M. Li, W. Zhu, D. Pan, H. Zhu and M. Liu, Facile synthesis of enzyme-embedded magnetic metal-organic frameworks as a reusable mimic multi-enzyme system: mimetic peroxidase properties and colorimetric sensor, *Nanoscale*, 2015, **7**, 18770–18779.
43 C. Y. Sun, C. Qin, X. L. Wang, G. S. Yang, K. Z. Shao, Y. Q. Lan, Z. M. Su, P. Huang, C. G. Wang and E. B. Wang, Zeolitic imidazolate framework-8 as efficient pH-sensitive drug delivery vehicle, *Dalton Trans.*, 2012, **41**, 6906–6909.
44 I. B. Vasconcelos, T. G. Da Silva, G. C. G. Militão, T. A. Soares, N. M. Rodrigues, M. O. Rodrigues, N. B. Da Costa, R. O. Freire and S. A. Junior, Cytotoxicity and slow release of the anti-cancer drug doxorubicin from ZIF-8, *RSC Adv.*, 2012, **2**, 9437–9442.
45 K. S. Park, Z. Ni, A. P. Cote, J. Y. Choi, R. Huang, F. J. Uribe-Romo, H. K. Chae, M. O'Keeffe and O. M. Yaghi, Exceptional chemical and thermal stability of zeolitic imidazolate frameworks, *Proc. Natl. Acad. Sci.*, 2006, **103**, 10186–10191.
46 C. Li, Y. He, L. Zhou, T. Xu, J. Hu, C. Peng and H. Liu, Fast adsorption of methylene blue, basic fuchsin, and malachite green by a novel sulfonic-grafted triptycene-based porous organic polymer, *RSC Adv.*, 2018, **8**, 41986–41993.
47 L. D. O'Neill, H. Zhang and D. Bradshaw, Macro-/microporous MOF composite beads, *J. Mater. Chem.*, 2010, **20**, 5720.
48 M. Das, N. Sanson, D. Fava and E. Kumacheva, Microgels loaded with gold nanorods: photothermally triggered volume transitions under physiological conditions, *Langmuir*, 2007, **23**, 196–201.
49 B. Sanz, C. von Bilderling, J. S. Tuninetti, L. Pietrasanta, C. Mijangos, G. S. Longo, O. Azzaroni and J. M. Giussi, Thermally-induced softening of PNIPAm-based nanopillar arrays, *Soft Matter*, 2017, **13**, 2453–2464.